

# Research on the Feasibility of Polyethylene terephthalate Foam Used in Wind Turbine Blades

Haiming Liu<sup>1</sup>, Maxwell Fordjour Antwi-Afari<sup>3</sup>, Haoyang Mi<sup>2\*</sup>, Chuntai Liu<sup>1,2\*</sup>

<sup>1</sup>School of Materials Science and Engineering, Zhengzhou University, Zhengzhou, Henan, PR China

<sup>2</sup>Key Laboratory of Materials Processing & Mold, Ministry of Education; National Engineering Research Center for Advanced Polymer Processing Technology, Zhengzhou University, Zhengzhou, Henan, PR China

<sup>3</sup>Department of Civil Engineering, College of Engineering and Physical Sciences, Aston University, Birmingham, B4 7ET, United Kingdom

## Correspondence

<sup>1</sup>**Haoyang Mi**, Key Laboratory of Materials Processing & Mold, Ministry of Education; National Engineering Research Center for Advanced Polymer Processing Technology, Zhengzhou University, Zhengzhou, Henan, PR China

Email: mihaoyang@zzu.edu.cn

<sup>2</sup>**Chuntai Liu**, School of Materials Science and Engineering, Zhengzhou University, Zhengzhou, Henan, PR China.

Key Laboratory of Materials Processing & Mold, Ministry of Education; National Engineering Research Center for Advanced Polymer Processing Technology, Zhengzhou University, Zhengzhou, Henan, PR China.

Email: ctliu@zzu.edu.cn

## Abstract

The sandwich foam materials of wind turbine blades are mainly polyvinyl chloride (PVC) and styrene-acrylonitrile (SAN) foams due to their good mechanical properties. However, PVC foam is unrecyclable and not resistant to high temperature conditions, whilst SAN foam is more expensive than PVC foam. Polyethylene terephthalate (PET) has irreplaceable advantages than both PVC and SAN foams because of

This article has been accepted for publication and undergone full peer review but has not been through the copyediting, typesetting, pagination and proofreading process which may lead to differences between this version and the [Version of Record](#). Please cite this article as doi: [10.1002/ep.13956](https://doi.org/10.1002/ep.13956)

its better mechanical performance, fantastic heat-resistant, low cost, and environmental friendliness (100 % recyclability). In this paper, the mechanical properties, thermal stability, resin uptake, and cellular morphology of PET T92, PVC H60, and SAN T400 foams were discussed. The results showed that the mechanical properties of T92 were equivalent to the existing H60 and T400, and even exceed their properties. It was found that the thermal stability of T92 was better than H60 and T400 under the same high temperature. Moreover, the pore of T92 was more uniform and regular than H60 and T400. Furthermore, the overall cost of T92 was lower than H60 and T400. The findings suggest that PET foam with a density of 100 kg/m<sup>3</sup> can completely replace PVC 60 kg/m<sup>3</sup> and SAN 71 kg/m<sup>3</sup> foams from the perspective of mechanical performance, cost, thermal stability, and environmental protection.

**KEYWORDS:**

wind turbine blades, PET foam, mechanical properties, thermal stability, environmental friendliness.

## 1 INTRODUCTION

In recent years, wind power is one of the most important renewable energy sources in the world. It is produced by using wind generators to harness the kinetic energy of wind, scale energy source, and electric power generated by wind turbines. It is reported that wind power is gaining worldwide popularity with globally installed capacity growing at an average annual rate of 25 % over the past decade.<sup>1</sup> Additionally, wind power provides 15 % of Europe's generation.<sup>2</sup> In 2020, around 96.3 GW of new wind power capacity was installed globally, representing the prime year in the history of bringing global cumulative wind power capacity up to 747.3 GW.<sup>3</sup> Modern wind turbine blades are one of the most basic and key components of wind-driven generators. It plays an important role in the power generation efficiency and operation safety of wind turbines and determines how much energy can be generated. The real wind blades and wind turbine blade construction are shown in Figures 1 (A) and (B),<sup>4,12</sup> respectively.

With the development of large wind turbine blades, new requirements on blade weight, quality, cost, and material consistency are put forward in the future. One of the most important raw materials for wind

turbine blades is the sandwich core, which is 15-20 % of the total cost of blade materials. It is mainly used in the leading edge, trailing edge, and shear web of wind turbine blades to reduce the weight of the blade. The sandwich core structure is usually used to increase the stiffness of the wind turbine blade structure to prevent local instability, blade buckling, whilst improving the load resistance of the wind turbine blade. The core material properties concerned with wind turbines are tensile, compression, shear, and peel. The sandwich core materials should meet the following characteristics: (1) mechanical properties should meet the requirements of wind turbine blade design parameters; (2) small specific gravity; (3) fantastic temperature resistance; (4) excellent chemical corrosion resistance; (5) outstanding compatibility with infusion resin; (6) low cost; and (7) environmentally friendly.<sup>5</sup>

Wind turbine blades are made of sandwich composite structures in which the core materials are combined with glass fiber and resin.<sup>6-8</sup> Traditionally, in the sandwich composites, lightweight polyvinyl chloride (PVC) foam and styrene-acrylonitrile (SAN) foam are often used as the core materials in wind turbine blades,<sup>9-12</sup> sandwiched between two continuous fiber-reinforced composite skins. PVC foam is a closed-cell with a cross-linked structure and mainly comes from DIAB and Maricell. SAN foam performs in similar production and properties with cross-linked PVC foam and can only be produced by using Gurit, which is foamed by compression molding of both PVC and SAN foams, which are characterized as thermoset materials and cannot be recycled.<sup>13-15</sup>

Based on data from General Electric renewable energy, in 2020, the average length of onshore wind turbine blades is about 70-90 m long, and the largest offshore wind turbine in the world is the Haliade-X 12-MW offshore wind turbine with a tower height of 160 m and rotor blades of 110 m long.<sup>16</sup> With the continued development of wind energy, the manufacturing length and curing temperature of wind turbine blades keep increasing to speed up the production efficiency. However, since PVC foam is not resistant to high temperature conditions during the manufacturing process of wind turbine blades, the phenomenon of PVC foam discoloration or even burning is often caused by an exothermic peak of resin (above 90 °C),

which will directly affect the performance of the blades. Although SAN foam possesses good temperature resistance, it is more expensive, inefficient, and unrecyclable, therefore, a new sandwich core material with better mechanical performance, fantastic heat-resistant, low cost, and environmental friendliness is urgently needed to replace PVC and SAN foams.

As a new type of thermoplastic engineering plastic, Polyethylene terephthalate (PET) foam has been developed to respond to the growing needs of structural core materials with excellent mechanical properties, outstanding high process temperature, and fantastic chemical resistance. Additionally, PET foam is compatible with wind energy, which aims to reduce its footprint and reinforce overall goals of waste reduction because of its 100% recyclability and low cost. Meanwhile, it can reduce the emissions of CO<sub>2</sub> during production, thus, it has irreplaceable advantages compared to both PVC and SAN foams.<sup>17,18</sup>

With the increasing pressure to reduce the cost, wind turbine blade manufacturers have General Electric, Siemens Gamesa, LM Wind Power, Goldwind, Envision, Sinoma, etc. However, there is almost no relevant literature on how PET foam can be replaced by PVC and SAN foams for wind blades.

PET foam is manufactured by using thermoplastic polyethylene terephthalate, which results in a thermoplastic foam. It can be continuously extruded by a twin-screw extruder and is not only compatible with all types of liquid thermosetting resin, adhesive bonding, and prepreg but also with vacuum infusion, compression molding, and thermoforming.<sup>19,20</sup> However, to increase its mechanical properties as much as possible, it is favorable to turn the foam in the perpendicular direction of the sheet. This can be achieved by welding the sheets together and then cutting them up to desired sheet thicknesses. The processes of PET foam extrusion and welding are shown in Figure S1. PET foam is a physical foaming, which is more uniform, stable, and has good compatibility. Consequently, it is very suitable for the production process of wind blades. PVC and SAN foams are chemical foamings, which are characterized as being inefficient, expensive, unrecyclable, and environmentally unfriendly.

The mechanical properties of foam are very important for wind blades design, therefore, to measure whether PET foam could replace PVC and SAN foams, these mechanical properties are the crucial factors. Before 2015, a blade production cycle is normally 48 h. To improve the blade production efficiency, the blade production cycle is now 32-36 h, and can even achieve 24 h per blade soon to meet the requirements of the blade production process. In addition, the curing temperature would be gradually rising, indicating that the heat resistance of foam is also a very significant factor. In a sandwich composite, resin uptake is the amount of resin absorbed by the core and the composite face skins. Minimizing resin uptake of wind turbine blades plays an essential role in reducing the weight of wind turbine blades.<sup>21-23</sup> It has been demonstrated that a lower resin uptake might help to increase stability and stiffness of a blade, reduce cost, and ultimately reduce the Levelized Cost of Energy.<sup>24, 25</sup>

Given the above, the ultimate goal of this study is to find a new sandwich foam material with better mechanical performance, fantastic heat-resistant, low cost, and environmental friendliness to replace PVC and SAN foams. In the present study, we focused on the application of PET foam with a density of 100 kg/m<sup>3</sup> in wind turbine blades, whilst the mechanical properties, thermal stability, and resin uptake of the three types of foams are compared. It is necessary to develop PET foam with low density and high performance for wind turbine blades. Moreover, PET foam needs continuous improvement and an increase in its overall performance in the future.

## **2 MATERIALS AND METHODS**

### **2.1 Materials**

Table S1 summarizes the detailed information of PVC H60, SAN T400, and PET T92, including manufacturer, country, color, density, and applicable temperature of three kinds of foams. An epoxy infusion resin system was used with a density of 1.10 g/cm<sup>3</sup> (Swancor 2511-1A/BS, resin: hardener = 100:30±5, weight ratio). Biaxial fabric with an aerial weight of 808 g/m<sup>2</sup> was used (CPIC). The structural

adhesive used to bond samples to test mechanical properties was supplied by 3M DP 460 NS. All auxiliary materials for vacuum infusion were provided by Airtech. They include peel plies (R85PA66), release films (W1300), vacuum sealant tapes (WD209), resin flow meshes (VI160W), resin flow channels (PA11-PHL 14×1mm), and vacuum bagging films (WRIGHTLON® 7400, CF).

## 2.2 Characterization

The core in the sandwich structure resisted the shear, compression, tensile, and peel stress during different times and locations in the applications of wind blades. The shear stress on the core was parallel to the surface while the compression and tension stresses were perpendicular to the surface.<sup>26</sup> All samples were tested at room temperature and humidity. The mechanical properties of testing the samples were characterized by using the Zwick/Roell Z100 (BT1-FR100THW.A2K). The thermal stability of the foam was directly related to the processing of wind turbine blades during production. The foam's resin uptake was related to the cost and could improve the mechanical properties of wind blades.

## 2.3 Density measurement

The density of the foam was tested according to ISO 845.<sup>27</sup> It was not used to describe the mechanical performance of the material, however, in structural design, it was rated as a very important property of the material. The density  $\rho$  (apparent overall density or apparent core density) of the test specimen, in grams per cubic centimeters ( $\text{g}/\text{cm}^3$ ), was given by the formula:

$$\rho = \frac{m}{v} \quad (1)$$

where,  $m$  is the mass, in grams (g), of the test specimen;  $v$  is the volume, in cubic centimeters ( $\text{cm}^3$ ), of the test specimen.

## 2.4 Tensile properties

The tensile properties were tested according to ASTM C297 with more than six specimens per series to generate six effective data, tensile strength, and tensile modulus,<sup>28</sup> which were determined by using an

extensometer. Tensile strength was calculated by using the maximum load, which normally occurred when the specimen breaks. Tensile modulus was calculated by using the steepest part of the load-displacement curve in the elastic region. Figure S2 shows the tensile load applied to a composite material.

Ultimate strength - The calculation of the ultimate flatwise tensile strength was given by the equation:

$$F_z^{fu} = \frac{P_{max}}{A} \quad (2)$$

where,  $F_z^{fu}$  is the ultimate flatwise tensile strength, MPa [psi];  $P_{max}$  is the ultimate force prior to failure, N [lbf], and  $A$  is the cross-sectional area, mm<sup>2</sup> [in.<sup>2</sup>].

## 2.5 Compression testing

The compressive properties were tested according to ISO 844 with more than six specimens per series to generate six effective data,<sup>29</sup> compressive strength, and compressive modulus which were determined by using an extensometer. Compressive strength was calculated at maximum load or 10% deflection. If the material undergoes a deformation higher than 10 %, it could be required to report the stress at 10 % as the compressive strength. Compressive modulus was calculated from the linear part of the load-displacement curve in the elastic region. Figure S3 illustrates a composite under a compressive load.

The compressive strength  $\sigma_m$  was given, in kilopascals, by the equation:

$$\sigma_m = 10^3 \times F_m / A_0 \quad (3)$$

where,  $F_m$  is the maximum force reached, in newtons;  $A_0$  is the initial cross-sectional area, in square meters, of the test specimen.

The compressive stress at 10 % relative deformation  $\sigma_{10}$  was given, in kilopascals, by the equation:

$$\sigma_{10} = 10^3 \times F_{10} / A_0 \quad (4)$$

where,  $F_{10}$  is the force, in newtons, corresponding to a relative deformation of 10%.

The compressive modulus of elasticity  $E$ , in kilopascals, was calculated from the equations:

$$E = \sigma_e \times h_0 / x_e \quad (5)$$

and

$$\sigma_e = 10^3 \times F_e / A_0 \quad (6)$$

where,  $F_e$  is the force at the end of the conventional elastic zone (a well-defined straight portion of the force- displacement curve), in newtons;  $x_e$  is the displacement at  $F_e$ , in millimeters;  $h_0$  is the initial thickness, in millimeters, of the test specimen.

## 2.6 Shear properties

The shear properties were tested according to ASTM 273 with more than six specimens per series to generate six effective data shear strength, shear modulus,<sup>30</sup> and shear strain, which were determined by using an extensometer. Shear strength was calculated at maximum load, core materials with a high elongation that yield more than 2 % offset method for the yield strength calculation. Shear modulus was calculated from the linear part of the load-displacement curve in the elastic region. Figure S4 showed a composite under a shear load.

Shear stress - The calculation of the instantaneous core shear stress was given as follows:

$$\tau = P / (L \cdot b) \quad (7)$$

where,  $\tau$  is the core shear stress, MPa [psi];  $P$  is the instantaneous force on the specimen, N [lbf];  $L$  is the length of the specimen, mm [in.], and  $b$  is the width of the specimen, mm [in.].

Engineering shear strain - The calculation of the instantaneous effective core shear strain was given as follows:

$$\gamma = u / t \quad (8)$$

where,  $\gamma$  is the core engineering shear strain, mm/mm [in./in.];  $u$  is the instantaneous displacement between loading plates, mm [in.], and  $t$  = thickness of the core, mm [in.].

Core Shear Modulus - The calculation of the effective core shear modulus was given as follows:

$$G = (\Delta P / \Delta u) t / (L \cdot b) \quad (9)$$



where,  $\Delta P/\Delta u$  is the slope of the force-displacement curve, in N/mm [lbf/in.], from 0.002 mm/mm to 0.006 mm/mm effective engineering shear strain.

## 2.7 Fracture Toughness Peel

The peel property was tested according to ASTM D1781 with more than six specimens per series to generate six effective data to determine the average peel strength.<sup>31</sup> The fracture toughness test was used to determine the cleavage strength of a composite skinned cored laminate. The composite skin was peeled away from the clamped core material and then returned to its starting point. The peel energy was calculated by considering the area under the loading curve so that the energy applied to bend the skin could be taken out from the total force due to failure of the samples. The peel strength was then taken as the energy in Joules required to cause failure of the core/skin interface, divided by the delamination area.

The average peel torque,  $T$ , was calculated by using the following equation:

$$T = [(F_p - F_o) (r_o - r_i)] / W \quad (10)$$

where,  $T$  is the average peel torque, mm·kg/mm (in·lb/in.) of width;  $r_o$  is the radius of flange, including one half of the thickness of the loading straps, mm (in.);  $r_i$  is the radius of the drum plus one half of the thickness of the adherend being peeled, mm (in.);  $F_p$  is the average load required to bend and peel adherend plus the load required to overcome the resisting torque, kg (lb);  $F_o$  is the load required to overcome the resisting torque, in pounds;  $W$  is the width of the specimen, in mm (in.).

## 2.8 Thermal stability

Thermal stability of H60, T400, and T92 was tested to investigate the mechanical properties of PET T92 foam at high temperature conditions. The test temperature is determined according to the actual heat resistance temperature of the three kinds of foams. The dimensions of the foam specimens were  $300 \times 300 \times 25$  mm and  $300 \times 300 \times 50$  mm without chamfer. The size of the samples was determined to meet the requirements of compressive, tensile, and shear tests at high temperature conditions. The samples were

put into an oven and baked at different temperature conditions (100 °C, 120 °C, and 150 °C) for 1 hour, respectively. Afterward, the samples were taken out and cooled at a room temperature to observe the surface color of the samples. Notably, the mechanical properties at different temperature conditions were also tested.

## 2.9 Resin uptake

Resin uptake in this present study was defined as the weight of resin absorbed by the exposed surface area of the core during infusion, expressed in kg/m<sup>2</sup>. The dimension of the foam specimens was 500 × 400 × 25 mm, three specimens per series to generate three effective data. The layout of the laminate used in the resin uptake test was shown in Figure S5. We removed the glass fibers and auxiliary materials on the foam surface after curing. The weight and dimensions of the core before and after infusion were measured, respectively.<sup>32-34</sup> Resin uptake was calculated by using this formula:

$$RU = (W_{inf} - W_{core}) / A_{exposed} \quad (11)$$

where,  $RU$  is resin uptake, %,  $W_{inf}$  is the weight of the core block before infusion, kg,  $W_{core}$  is the total weight of the core block after infusion (with resin absorbed in surface exposed to infusion), kg, and  $A_{exposed}$  is the total exposed surface area of the core block, m<sup>2</sup>.

## 2.10 Cellular morphology

The cellular morphology of the foam samples was characterized by using the Scanning electron microscopy (SEM) (TESCAN YEGA II, TESCAN s.r.o) at an acceleration voltage of 10 kV. The cryogenic broken samples were sputtered with a 13 nm gold layer by using a Sputter Coater 108auto (Cressington, Watford, England). The gold used was of 99.9 % purity. The magnification ratio was 100× for observing porous morphology. Pore density was analyzed by using a software image tool and calculated by using these formulas:<sup>35-37</sup>

$$N_c = \left(\frac{n}{A}\right)^{3/2} \cdot \varphi \quad (12)$$

$$\varphi = \frac{\rho_u}{\rho_f} \quad (13)$$

where,  $N_c$  is pore density (pore/cm<sup>3</sup>),  $n$  is pore amount within statistical areas,  $A$  is statistical areas in SEM photo (cm<sup>2</sup>),  $\varphi$  is the foaming expansion ratio of polymer,  $\rho_f$  is foamed density (g/cm<sup>3</sup>),  $\rho_u$  is unfoamed density (g/cm<sup>3</sup>).

### 3 RESULTS AND DISCUSSION

Aerodyn, WE4CE, Wind-Novation, and Sinoma are the four main famous wind turbine blade design companies in the world. The requirements on the mechanical properties of sandwich core material from wind blade design companies are listed in Table 1. As shown in Table 1, the mechanical properties of sandwich foam met the design requirements, as such, the sandwich foam could be used in most wind turbine blades. The main mechanical properties were tensile, compression, shear, and peel, however, other factors also need to be considered such as cost, foam thermal stability, blade weight, resin uptake, and so on. In general, PET foam with a density of 100 kg/m<sup>3</sup> is the best choice to replace PVC (60 kg/m<sup>3</sup>) and SAN (71 kg/m<sup>3</sup>) foams for wind turbine blades.

#### 3.1 Mechanical properties

Since the current density of PVC foam used for wind turbine blades was mainly 60 kg/m<sup>3</sup> and SAN foam was 71 kg/m<sup>3</sup>, to meet the mechanical properties and cost advantages of wind turbine blades, the blade design company could use PET foam with a density of 100 kg/m<sup>3</sup> to replace PVC and SAN foams. The compression, shear, tensile, and peel performance of H60, T400, and T92 were tested at room temperature (25 °C), and the results were presented in Table 2. After the comparison between the three kinds of foams, it could be seen that all the mechanical property values of T92 were higher than the other two foams, except for the shear elongation at breakpoint. The average shear elongation of T92 (21.59 %) was higher than H60 (19.94 %) but lower than T400 (25.78 %) under the same test conditions. Despite these results, it still met all the requirements of the blade design companies. Therefore, T92 could completely replace

H60 and T400 from the perspective of wind blade mechanical performance design (the same density foam from different companies had similar mechanical properties).

### 3.2 Thermal stability

As the length of wind turbine blades continues to increase and improve efficiency, the curing temperature of wind blades would also increase. The temperature used for PVC foam in wind turbine blades was lower than 90 °C. As such, it was lower than 120 °C and higher than 150 °C for SAN foam and PET foam, respectively. However, during the wind turbine blades manufacturing process, the exothermic peak of resin could reach 100 °C or even higher (it could reach 150 °C under the infusion channel occasionally), and the time of resin exothermic peak can last for nearly 1 hour. The color of PVC foam changed from yellow to brown under high temperature (>90 °C), as shown in Figure 2. The changes in colors could directly affect the appearance and performance of the blades, which are unacceptable for the quality of wind turbine blades.

The thermal stability of H60, T400, and T92 was tested under different high temperature conditions (100 °C, 120 °C, and 150 °C). The results are shown in Table 3 and Figure 3. After the comparison of the three types of foams, it was found that the color of H60 changed from yellow to brown after 100 °C for 1 hour. With the increase in temperature, the color became darker and darker. T400 had a slight turn than before at 150 °C for 1 hour. Optimistically, it had almost no effect on T92 under the same high temperature (Remark: the color of the pictures had some chromatic aberration due to the light, however, it didn't affect the conclusion).

The mechanical properties of H60 at different high temperature conditions are shown in Figure 3. It was found that with an increase in temperature, the properties of compression, tensile, and shear of H60 gradually decreased. As compared to H60 at room temperature (25 °C), the compressive strength and modulus of H60 were reduced by 4 % and 4.64 %, 8 % and 8.62 %, and 17 % and 20.36 % at 100 °C,

120 °C, and 150 °C, respectively. The tensile strength and modulus of H60 had little effect at high temperature, which were reduced by 0.47 % and 0.16 %, 1.9 % and 2.16 %, and 3.79 % and 3.41 % at 100 °C, 120 °C, and 150 °C, respectively. The most influential mechanical properties such as shear strength and modulus were reduced by 5 % and 7.08 %, 10 % and 16.9 %, and 21.25 % and 30.28 % at 100 °C, 120 °C, and 150 °C, respectively. This is because PVC H60 foam is unstable in the presence of light and heat. When exposed to a temperature higher than 100 °C or the sun for a long time, it would decompose hydrogen chloride and change color. At higher temperature conditions, it would further autocatalytically decompose, eventually leading to molecular chain scission and decrease in mechanical properties. The key conclusion was that the degradation of the mechanical properties of H60 was very severe under high temperature conditions. Figure 4 showed the mechanical properties of T92 at different high temperature conditions. As expected, the compression, shear, and tensile performance of T92 hardly changed with increasing temperature. This is because the melting point of T92 is higher than 250 °C. When the temperature was below 150 °C, it wasn't high enough to significantly change the molecular chain mobility of T92, thus showing a negligible effect. Therefore, the thermal stability of T92 was better than H60 and T400, thus, very suitable for the production process of large wind turbine blades.

### **3.3 Resin uptake**

Resin uptake was an important factor to measure the cost of wind blades. The lower the resin absorption, the lower the manufacturing cost. The three types of foams introduced in this paper were all closed-cell foams. The pore size and depth can influence the absorption of resin, thus, the larger the pore size, the greater the resin uptake. Table 4 shows a summary of the resin uptake results of H60, T400, and T92 under the same testing condition. It was revealed that the average resin uptake value of T92 was 18.86 % higher than H60, and 12.26 % higher than T400.

### **3.4 Cellular morphology**

To further illustrate the relationships between the resin uptake and pores of the foams, the cellular morphology of H60, T400, and T92 were characterized by using Scanning electron microscopy (SEM). Figure 5 presents the SEM micrographs of the three types of foams in a magnification ratio of 100×. It was found that the cellular morphology of T92 was more uniform and regular than both H60 and T400. The pore size of T92 was smaller than both H60 and T400, whilst the number of pores of T92 was more than the other two foams through calculation and measurement. The average pore sizes of H60, T400, and T92 were 0.43 mm, 0.47 mm, and 0.4 mm, respectively. Similarly, the pore densities of H60, T400, and T92 were  $1.42 \times 10^5$  pores/cm<sup>3</sup>,  $2.51 \times 10^5$  pores/cm<sup>3</sup>, and  $2.42 \times 10^5$  pores/cm<sup>3</sup>, respectively.

Pore size distribution was a parameter to show the number of pores of different size ranges. It has been used by many researchers to investigate the relationship between porous structure and foam properties, especially compressive strength, thermal conductivity, and resin uptake.<sup>38</sup> As shown in Figure 5, the pore size of the three foams indicated a broad distribution and T92 was more uniform than the other two foams. For H60, its maximum pore size was around 0.7 mm. It was reported that the maximum pore sizes for T400 and T92 were around 0.8 mm and 0.6 mm, respectively. A summary of the pore size, number, and pore density of H60, T400, and T92 was provided in Table 5.

Theoretically, the smaller the pore size, the lower the resin uptake.<sup>39</sup> As indicated in Table 4 and Table 5, the pore size of H60 was smaller than T400, whilst the average resin uptake of H60 was lower than T400. However, the pore size of T92 was smaller than H60 and T400, whilst the resin uptake of T92 was higher than the other two foams. These results could be explained by the fact that the pore at the position of T92 welding line could be destroyed because of high temperature (above 250 °C) during welding, which could create holes. However, the results revealed that the pores of the welding line of T92 absorbed more resin after infusion. As presented in Figure 6, the cross-section of H60, T400, and T92 after infusion (T92

was the cross-section of the welding line), showed the blue ink on the surface of foam, where the epoxy resin mixed with dyestuff. Consequently, the section of welding line absorbed more blue resin.

The resin uptake of T92 was higher than H60 and T400, however, the price of T92 was 30-40% lower than H60, and 40-50 % lower than T400 according to the pricing of wind turbine blades for sandwich foam. Optimistically, the cost of the application of T92 was lower than H60 and T400 in wind turbine blades. Another advantage of using T92 was that it benefits the stiffness of blades because of its higher density and lower pore variability.<sup>40,41</sup>

#### **4 CONCLUSIONS**

In this paper, the application of PET foam with a density of 100 kg/m<sup>3</sup> in wind turbine blades was discussed. The compression, shear, tensile, peel, thermal stability and resin uptake performance of H60, T400, and T92 were tested under the same conditions.

The results demonstrated that the compressive strength and modulus, tensile strength and modulus, shear strength and modulus, and peel strength of T92 were equivalent to or even exceed that of the existing H60 and T400, thus, it could meet the requirements of wind turbine blade design companies.

The thermal stability of T92 was better than H60 and T400 under the same high temperature, indicating its suitability for the production process of wind turbine blades.

The pore of T92 was more uniform and regular than H60 and T400. It was found that pore size was smaller than the other two foams, whilst the resin uptake of T92 was higher than H60 and T400. Nonetheless, the overall cost of T92 was lower than both H60 and T400.

PET foam was a green and environmentally friendly material because of its 100 % recyclability. In addition, PET foam scraps during the production process, which could also be recycled and reused. From the perspective of environmental protection, PET foam had more advantages than both PVC and SAN foams for the application of wind turbine blades in the future.

The key conclusions were given based on current test results indicating that T92 could completely replace H60 and T400 from the perspective of mechanical performance, cost, and environmental protection. Similarly, PET foam with a density of  $100 \text{ kg/m}^3$  could replace PVC foam ( $60 \text{ kg/m}^3$ ) and SAN foam ( $71 \text{ kg/m}^3$ ) in all fields of wind turbine blades.

#### **ACKNOWLEDGEMENTS**

The authors would like to thank the financial support from the National Natural Science Foundation of China (52173049; 12072325), the National Key R&D Program of China (2019YFA0706802).

#### **AUTHOR CONTRIBUTIONS**

**Haiming Liu:** Conceptualization; data curation; investigation; formal analysis; methodology; resources; writing - original draft. **Maxwell Fordjour Antwi-Afari:** Writing - review and editing. **Haoyang Mi:** Conceptualization, supervision, funding acquisition; validation; project administration; writing - review and editing (equal). **Chuntai Liu:** Conceptualization, supervision, funding acquisition; formal analysis.

#### **DATA AVAILABILITY STATEMENT**

The data that support the findings of this study are available from the corresponding author upon reasonable request.

#### **ORCID**

Haiming Liu: <https://orcid.org/0000-0002-0307-1133>

Hao-Yang Mi: <https://orcid.org/0000-0002-0894-9371>



## REFERENCES

1. Anders Arvesen and Edgar G Hertwich. Corrigendum: Environmental implications of large-scale adoption of wind power: a scenario-based life cycle assessment. *ENVIRONMENTAL RESEARCH LETTERS*. 2012;7:039501. <https://doi.org/10.1088/1748-9326/7/3/039501>.
2. Wind power, Rapid growth of wind power is happening. <https://group.vattenfall.com/what-we-do/our-energy-sources/wind-power>
3. Businesswire, Brazil Wind Power Market to 2025 and the Impact of COVID-19- ResearchAndMarkets.com. 2020; AM Eastern Daylight Time. <https://www.businesswire.com/news/home/20200730005664/en/>
4. Shau-Tarng Lee; Polymeric Foams: *Innovations in Processes, Technologies, and Products*, 2016; 22(8): 264-283. ISBN 9781498738873.
5. Álvaro Cañadas-López, Diana Rade-Loor. Growth and Yield Models for Balsa Wood Plantations in the Coastal Lowlands of Ecuador. *Forests*. 2019; 10(8): 733. <https://doi.org/10.3390/f10090733>.
6. Huang CL, Lindström H, Nakada R, Ralston J. Cell wall structure and wood properties determined by acoustics - A selective review. *Holz Als Roh - Und Werkst*. 2003;61(5):321-335. <https://doi:10.1007/s00107-003-0398-1>.
7. Gibson LJ, Ashby MF. Cellular Solids: Structure and Properties. Second Edition. *Cambridge University Press*. 2014. <https://assets.cambridge.org/97805214/99118>.
8. Malakooti S, Zhao E, Tsao N, et al. Synthesis of aerogel foams through a pressurized sol-gel method. *Polymer (Guildf)*. 2020;208(122925):1-6. <https://doi.org/10.1016/j.polymer.2020.122925>.
9. Ma J, Hanan JC, Komanduri R, Lu H. Simulation of the deformation mechanisms of bulk metallic glass (BMG) foam using the material point method. *C - Comput Model Eng Sci*. 2012;86(4):349-384. <https://doi.org/10.3970/cmcs.2012.086.349>
10. Luo H, Zhang Y, Wang B, Lu H. Characterization of the compressive behavior of glass fiber reinforced polyurethane foam at different strain rates. *J Offshore Mech Arct Eng*. 2010;132(2):1-12. <https://doi.org/10.1515/epoly-2017-0072>.
11. Daphalapurkar NP, Hanan JC, Phelps NB, Bale H, Lu H. Tomography and simulation of microstructure evolution of a closed-cell polymer foam in compression. *Mech Adv Mater Struct*. 2008;15(8):594-611. <https://doi.org/10.1080/15376490802470523>.
12. Griffith DT, Ashwill TD. The Sandia 100-meter all-glass baseline wind turbine blade: SNL100-00. *Baseline*. 2011; 6:1-67. <https://energy.sandia.gov/wp-content/gallery/uploads/113779>.
13. Luong DD, Pinisetty D, Gupta N. Compressive properties of closed-cell polyvinyl chloride foams at low and high strain rates: experimental investigation and critical review of state of the art. *Compos Part B Eng*. 2013;44(1):403-416. <https://doi.org/10.1016/j.compositesb.2012.04.060>.
14. Griffith DT. SANDIA REPORT the SNL100-02 Blade: advanced core material design studies for the Sandia 100-meter blade. <http://www.ntis.gov/help/ordermethods.asp?loc=7-4-0#online>. Accessed April 7, 2021.
15. Griffith DT, Richards PW. The SNL100-03 blade: design studies with flatback airfoils for the Sandia 100-meter blade. Albuquerque, NM, and Livermore, CA (United States); 2014.
16. GE Renewable Energy. World's most powerful offshore wind turbine: Haliade-X 12 MW/*GE Renewable Energy*. Published 2020. Accessed October 2, 2020. <https://www.ge.com/renewableenergy/wind-energy/offshore-wind/haliade-x-offshore-turbine>.
17. Sloan J, et al. Core for composites: Winds of change. *Composites Technology*, 2010; 10. [https://www.researchgate.net/publication/295710573\\_Core\\_for\\_composites\\_Winds\\_of\\_change](https://www.researchgate.net/publication/295710573_Core_for_composites_Winds_of_change).
18. Sloan J, et al. Wind foam sources: PET, SAN & PVC. *Composites Technology*, 2010; 1. [https://www.researchgate.net/publication/295662679\\_Wind\\_foam\\_sources\\_PET\\_SAN\\_PVC](https://www.researchgate.net/publication/295662679_Wind_foam_sources_PET_SAN_PVC).
19. Ma, W. and Feichtinger, F. Polyester core materials and structural sandwich composites thereof. 2011. US Patent 7,951,449 assigned to Baltek Corporation. <https://www.freepatentsonline.com/7951449.html>.
20. Danisman, Murat, et al. Monitoring of resin flow in the resin transfer molding (RTM) process using point-voltage sensors. *Composites Science and Technology*. 2007; 67(3): 367-379. <https://doi.org/10.1016/j.compscitech.2006.09.011>.

21. Stoll F. Blade cost and weight reduction using TYCOR W engineering cores[C]/2010 Wind Turbine Blade Workshop. *Miamisburg, OH: WebCore Technologies.* 2010; 20-25. <https://www.windpower.sandia.gov/2010BladeWorkshop/PDFs/2-1-D-2-Stoll>.
22. Cairns D S , Shramstad J D . Evaluation of Hand Lay-Up and Resin Transfer Molding in Composite Wind Turbine Blade Manufacturing. *Office of Scientific & Technical Information Technical Reports.* 2000. <https://doi.org/10.2172/760737>.
23. Yao S, Chetan M, Griffith DT. Structural design and optimization of a series of 13.2MW downwind rotors. *Wind Eng January.* 2021;1-11. <https://doi.org/10.1177/0309524X20984164>.
24. Chen X. Fractographic analysis of sandwich panels in a composite wind turbine blade using optical microscopy and X-ray computed tomography. *Eng Fail Anal.* 2020;111(104475):1-12. <https://doi.org/10.1016/j.engfailanal.2020.104475>.
25. Majumdar P, Srinivasagupta D, Mahfuz H, Joseph B, Thomas MM, Christensen S. Effect of processing conditions and material properties on the debond fracture toughness of foam-core sandwich composites: experimental optimization. *Compos Part A Appl Sci Manuf.* 2003;34(11):1097-1104. [https://doi.org/10.1016/S1359-835X\(03\)00200-8](https://doi.org/10.1016/S1359-835X(03)00200-8).
26. Feichtinger, K. A . Test Methods and Performance of Structural Core Materials -1. Static Properties. *Journal of Reinforced Plastics & Composites.* 1989; 8(4):334-357. <https://doi.org/10.1177/073168448900800402>.
27. ISO International. ISO 845:2006(E) standard test method for cellular plastics and rubbers-Determination of apparent density. *International standard.* <https://www.iso.org/standard/39408.html>.
28. ASTM International. ASTM C297-61 standard test method for tensile strength of flat sandwich constructions in flatwise plane. *An American national standard.* <https://www.document-center.com/standards/show/ASTM-C297>.
29. ISO International. ISO 844:2007(E) standard test method for rigid cellular plastics-Determination of compression properties. *International standard.* <https://www.iso.org/obp/ui/#!iso:std:45078:en>.
30. ASTM International. ASTM C 273/C 273M-07a standard test method for shear properties of sandwich core materials. *An American national standard.* <https://webstore.ansi.org/Standards/ASTM/ASTMC273C273M07a>.
31. ASTM International. ASTM D 1781-98 standard test method for climbing drum peel for adhesives. *An American national standard.* <https://webstore.ansi.org/Standards/ASTM/ASTMD1781982012>.
32. Cao DY, Malakooti S, Kulkarni V N, et al. The effect of resin uptake on the flexural properties of compression molded sandwich composites. *Wind Energy,* 2021: 1-23. <https://doi.org/10.1002/we.2661>.
33. Diab Group. Divinycell PVC grooved & perforated core. *Tech Data Sheet.* 2014:1-2. <https://www.diabgroup.com/products-services/divinycell-pvc>.
34. Cao, D., Malakooti, S., Kulkarni, V.N. et al. Nanoindentation measurement of core–skin interphase viscoelastic properties in a sandwich glass composite. *Mech Time-Depend Mater* 25, 353–363 (2021). <https://doi.org/10.1007/s11043-020-09448-y>.
35. Naguib HE, Park CB, Reichelt N, Danzer U. Strategies for achieving ultra-low-density polypropylene foams. *Polym Eng Sci.* 2002; 1481-1492. <https://doi.org/10.1002/pen.11045>.
36. Xiangdong Wang, Wei Liu et al. Study on the effect of dispersion phase morphology on porous structure of poly (lactic acid)/poly (ethylene terephthalate glycol-modified) blending foams. *Polymer.* 2013; 54: 5839-5851. <https://doi.org/10.1016/j.polymer.2013.08.050>.
37. Liu Haiming, et al. The Preparation and Characterization of Branching Poly (ethylene terephthalate) and its Foaming Behavior. *Cellular Polymers.* 2015;34(2):63-94. <https://doi.org/10.1177/026248931503400202>.
38. Li DC, Liu T, Zhao L, Yuan WK. Foaming of linear isotactic polypropylene based on its non-isothermal crystallization behaviors under compressed CO<sub>2</sub>. *Polymer.* 2011; 60 (1): 89-97. <https://doi.org/10.1016/j.supflu.2011.07.015>.
39. Zhang P, Haag M, Kraft O, Wanner A, Arzt E. Microstructural changes in the cell walls of a closed-cell aluminium foam during creep. *Philos Mag A Phys Condens Matter, Struct Defects Mech Prop.* 2002; 82(16):2895-2907. <https://doi.org/10.1080/01418610208239623>
40. Saenz EE, Carlsson LA, Karlsson A. Characterization of fracture toughness (G<sub>c</sub>) of PVC and PES foams. *J Mater Sci.* 2011;46(9):3207-3215. <https://doi.org/10.1007/s10853-010-5205-x>
41. Redenbach C, Shklyar I, Andrä H. Laguerre tessellations for elastic stiffness simulations of closed foams with

strongly varying cell sizes. *Int J Eng Sci.* 2012; 50(1):70-78. <https://doi.org/10.1016/j.ijengsci.2011.09.002>

Accepted Article

## FIGURE CAPTION

**FIGURE 1** (A) The real wind turbine blades and (B) Wind turbine blade construction

**FIGURE 2** The temperature curve during the curing process of wind blades

**FIGURE 3** The mechanical properties of H60 at different high temperature conditions

(A) The compressive strength of H60; (B) The compressive modulus of H60; (C) The shear strength of H60; (D) The shear modulus of H60; (E) The tensile strength of H60; (F) The tensile modulus of H60;

**FIGURE 4** The mechanical properties of T92 at different high temperature conditions

(A) The compressive strength of T92; (B) The compressive modulus of T92; (C) The shear strength of T92; (D) The shear modulus of T92; (E) The tensile strength of T92; (F) The tensile modulus of T92;

**FIGURE 5** SEM micrographs and pore size distribution of the H60, T400, and T92

**FIGURE 6** The cross-section of H60, T400, and T92 after infusion curing

## TABLE CAPTION

**TABLE 1** The requirements of mechanical properties of sandwich foam from wind turbine blade design companies

**TABLE 2** Comparison of the mechanical properties of H60, T400 and T92 at room temperature (25 °C)

**TABLE 3** Thermal stability of three types of foams under different high temperature conditions

**TABLE 4** The resin uptake of H60, T400, and T92

**TABLE 5** Pore morphology data of H60, T400, and T92

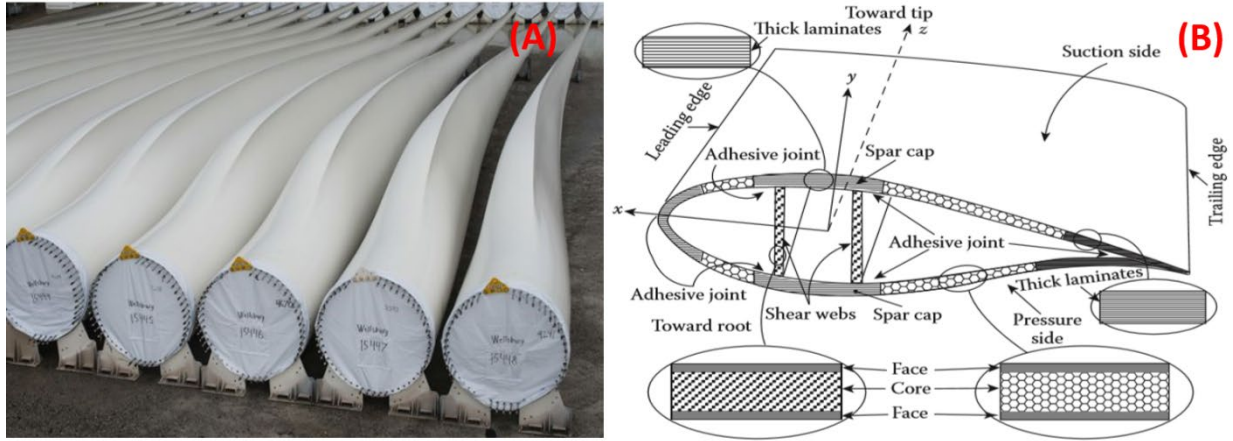


**FIGURE 1** (A) The real wind turbine blades and (B) Wind turbine blade construction

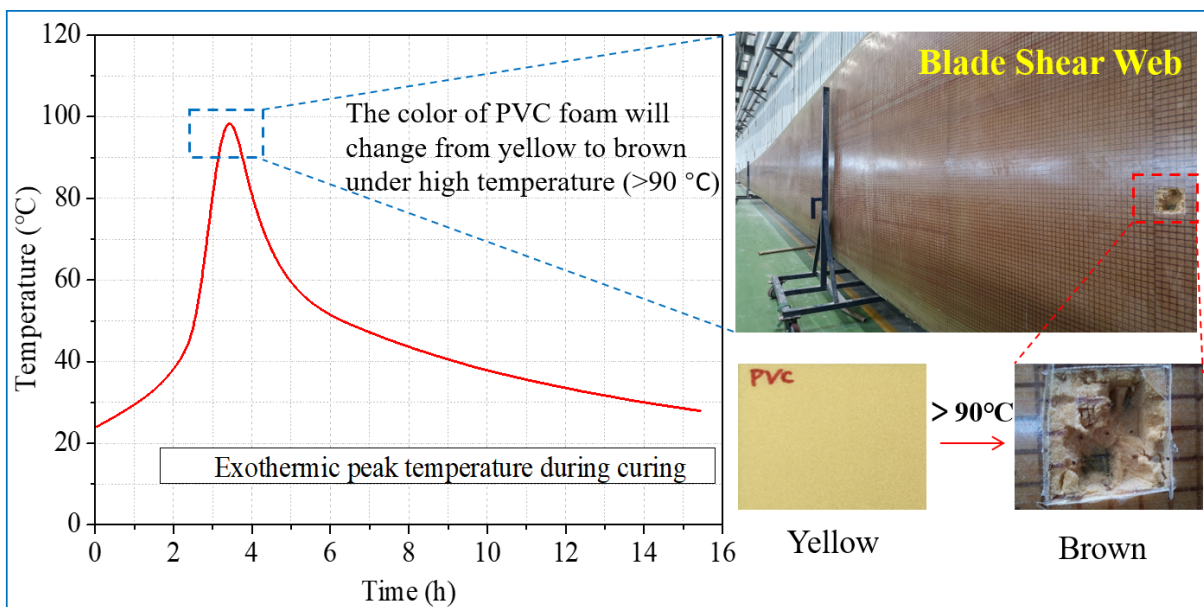


**FIGURE 2** The temperature curve during the curing process of wind blades



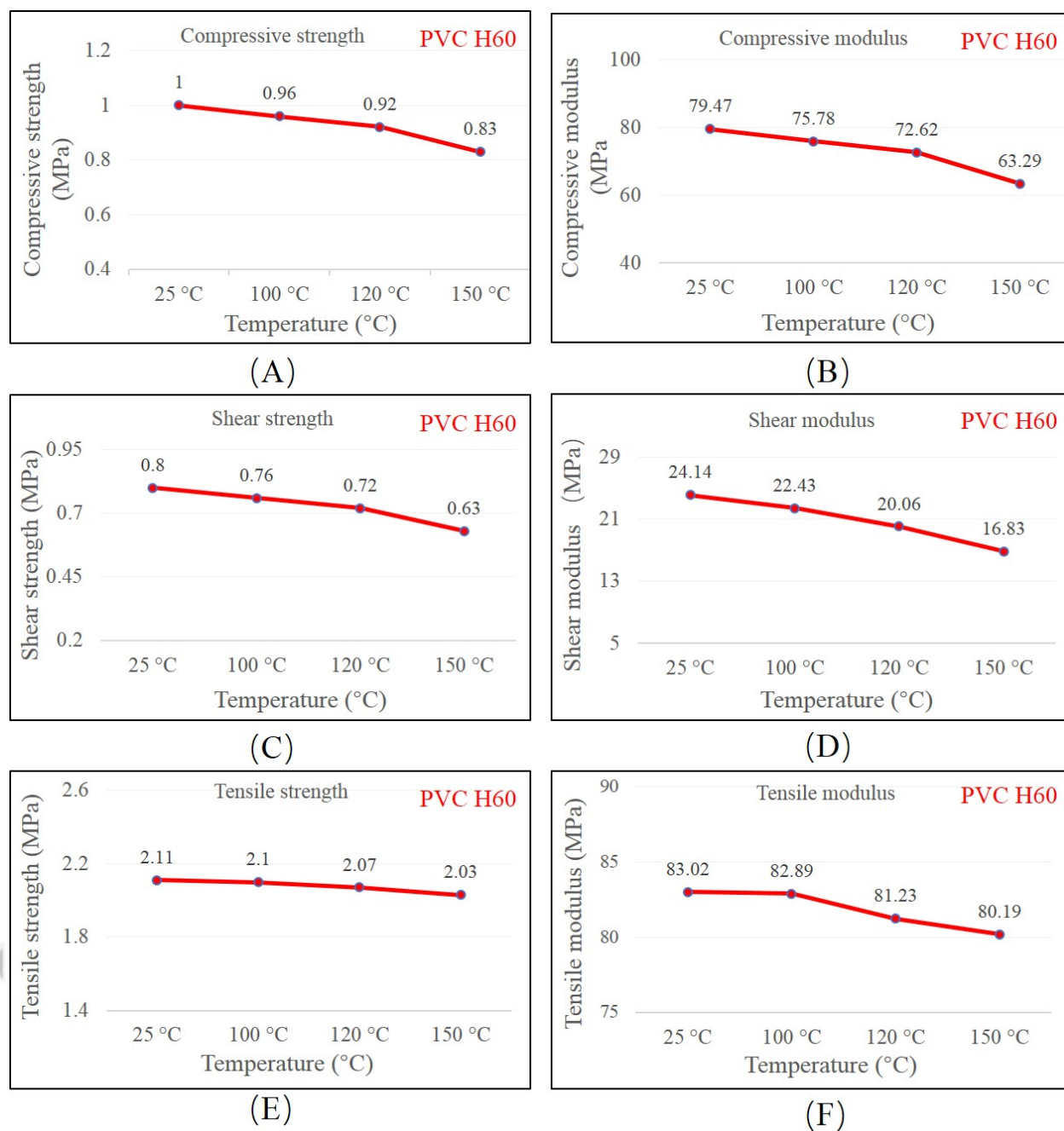
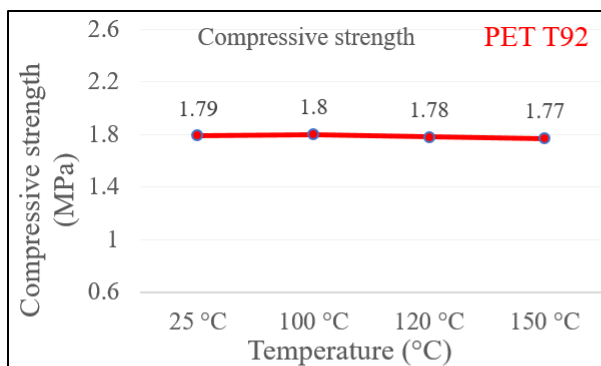
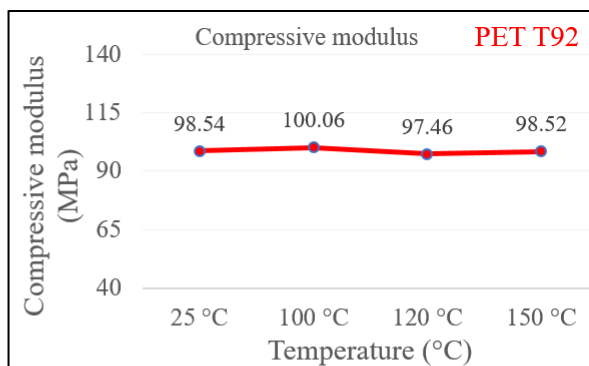


**FIGURE 3** The mechanical properties of H60 at different high temperature conditions

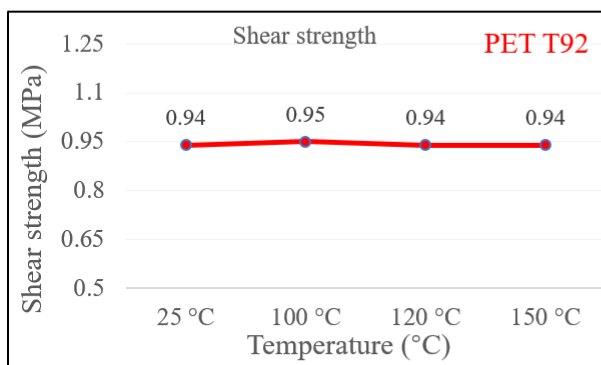
(A) The compressive strength of H60; (B) The compressive modulus of H60; (C) The shear strength of H60; (D) The shear modulus of H60; (E) The tensile strength of H60; (F) The tensile modulus of H60;



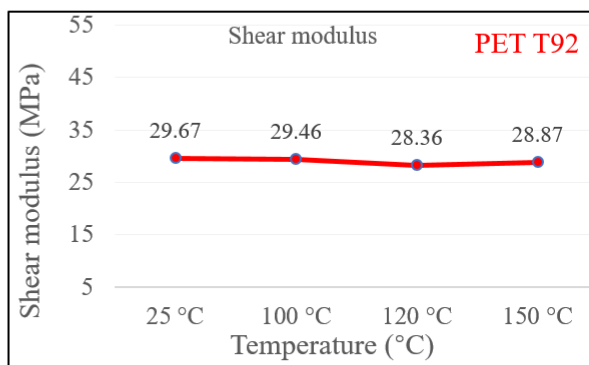
(A)



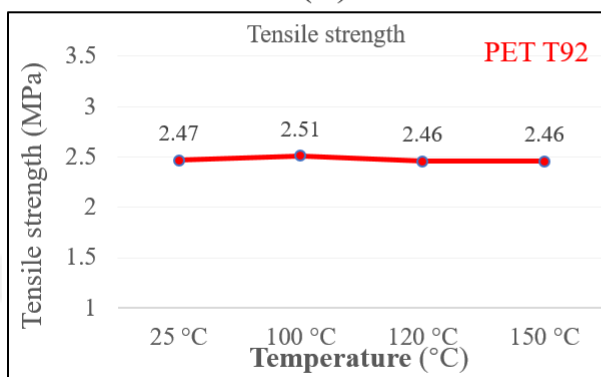
(B)



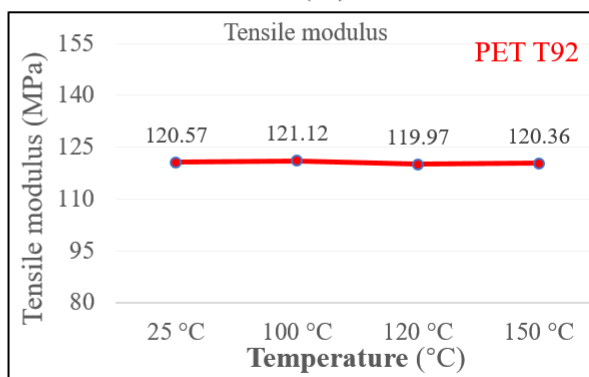
(C)



(D)



(E)



(F)

**FIGURE 4** The mechanical properties of T92 at different high temperature conditions

(A) The compressive strength of T92; (B) The compressive modulus of T92; (C) The shear strength of T92; (D) The shear modulus of T92; (E) The tensile strength of T92; (F) The tensile modulus of T92;



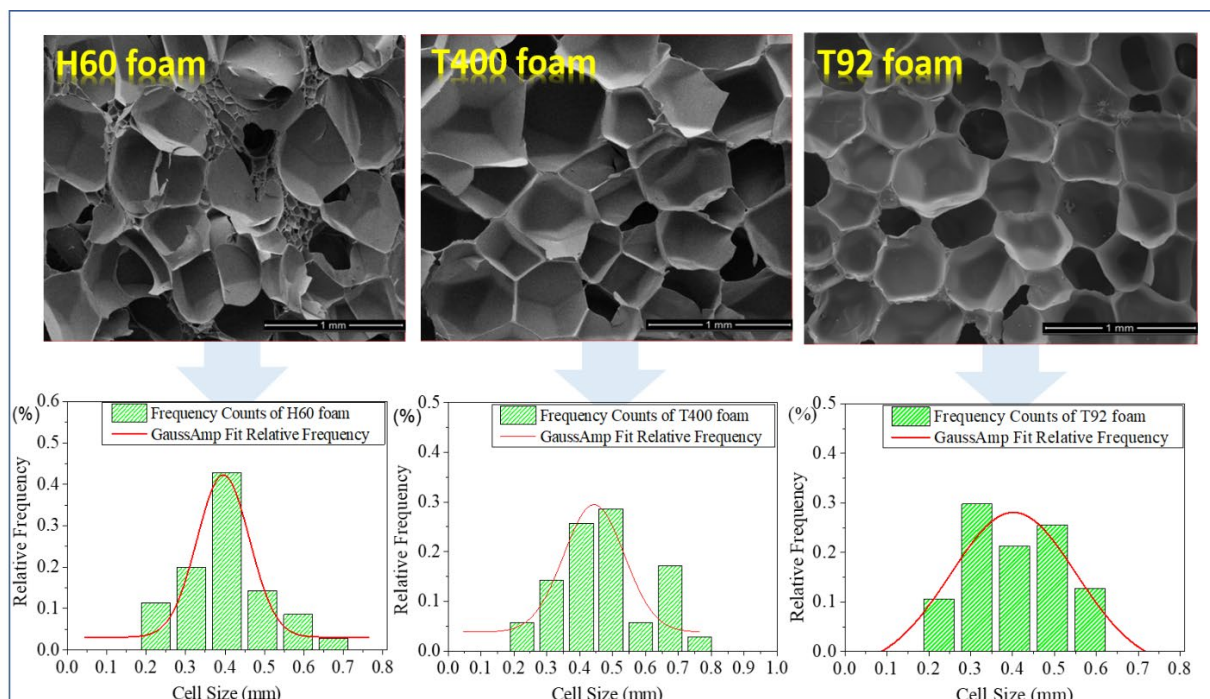


**FIGURE 5** SEM micrographs and pore size distribution of the H60, T400, and T92

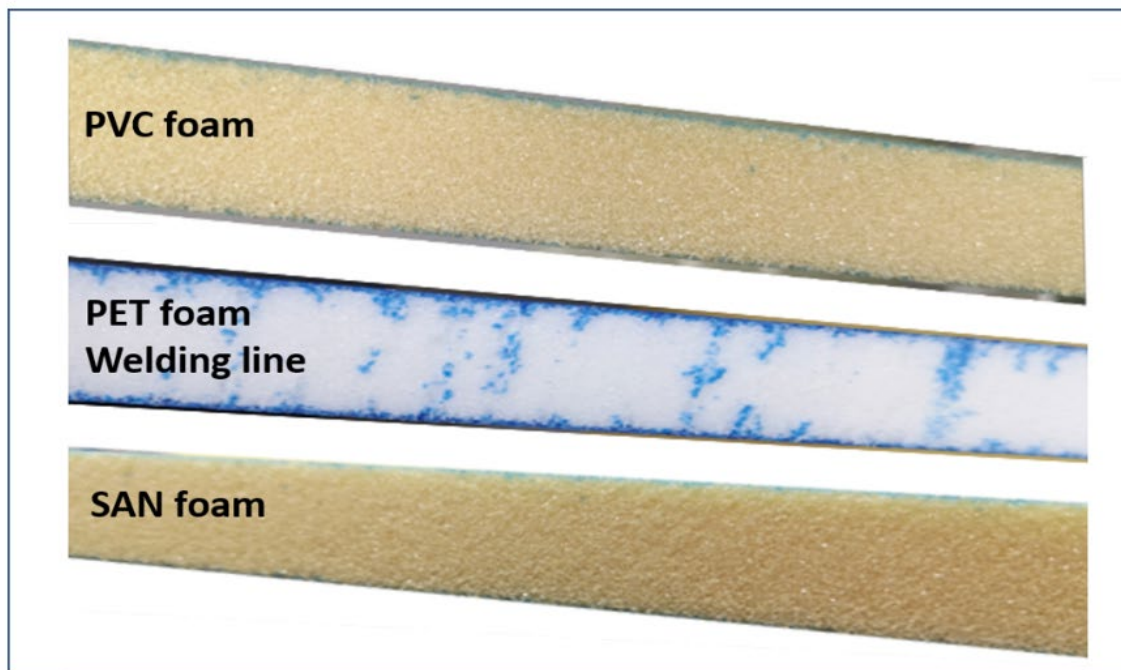


**FIGURE 6** The cross-section of H60, T400, and T92 after infusion curing

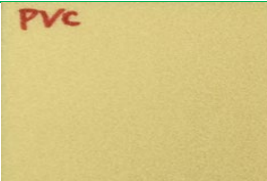
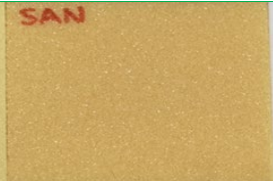
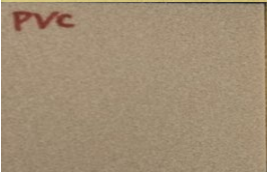
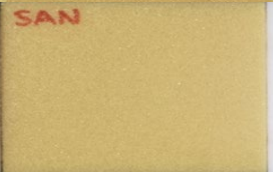
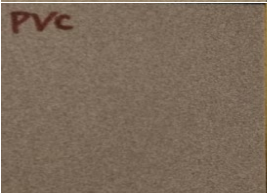
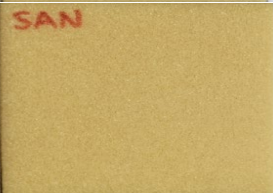
**TABLE 1** The requirements of mechanical properties of sandwich foam from wind turbine blade design companies

Items	Standards	Units	Wind turbine blade design companies			
			Aerodyn	WE4CE	Wind-Novation	Sinoma
Density	ISO 845	kg/m <sup>3</sup>	--	--	--	--
Tensile Strength	ASTM C297	MPa	--	>0.35 (Min Value)	--	>1.2 (Min Value)
Tensile Modulus	ASTM C297	MPa	--	>35 (Min Value)	--	>70 (Min Value)
Compressive strength	ISO 844	MPa	>0.65 (Min Value)	>0.35 (Min Value)	>0.62 (Min Value)	>0.65 (Min Value)
Compressive modulus	ISO 844	MPa	>58 (Min Value)	>35 (Min Value)	>42 (Min Value)	>65 (Min Value)
Shear Strength	ASTM C273	MPa	>0.6 (Min Value)	>0.23 (Min Value)	>0.5 (Min Value)	>0.6 (Min Value)
Shear Modulus	ASTM C273	MPa	>18 (Average Value)	>15 (Min Value)	>17 (Min Value)	>22 (Min Value)
Shear Elongation	ASTM C273	%	>4 (Average Value)	--	--	--
Peel strength	ASTM D1781	(N·mm) /mm	--	--	--	>20 (Min Value)

**TABLE 2** Comparison of the mechanical properties of H60, T400 and T92 at room temperature (25 °C)

Items	Standard	Unit	Series n=6	H60	T400	T92
Density	ISO 845	kg/m <sup>3</sup>	Ave	60.73	71.56	100.68
			Std. dev	0.5	0.72	0.45
Compressive strength	ISO 844	MPa	Ave	1.00	1.02	1.79
			Std. dev	0.02	0.04	0.02
Compressive modulus	ISO 844	MPa	Ave	79.47	61.20	98.54
			Std. dev	2.13	1.78	1.94
Shear Strength	ASTM C273	MPa	Ave	0.80	0.84	0.94
			Std. dev	0.03	0.02	0.06
Shear Modulus	ASTM C273	MPa	Ave	24.14	29.14	29.67
			Std. dev	1.12	1.31	1.16
Shear Elongation at break	ASTM C273	%	Ave	19.94	25.78	21.59
			Std. dev	2.49	2.26	3.94
Tensile Strength	ASTM C297	MPa	Ave	2.11	1.58	2.47
			Std. dev	0.1	0.06	0.29
Tensile Modulus	ASTM C297	MPa	Ave	83.02	91.55	120.57
			Std. dev	2.65	1.37	6.29
Peel strength	ASTM D1781	(N·mm)/mm	Ave	24.98	31.85	42.83
			Std. dev	2.1	2.1	2.94

**TABLE 3** Thermal stability of three types of foams under different high temperature conditions

Testing condition	H60	T400	T92
25 °C	 PVC	 SAN	 PET
100 °C for 1 hour	 PVC	 SAN	 PET
120 °C for 1 hour	 PVC	 SAN	 PET
150 °C for 1 hour	 PVC	 SAN	 PET

**TABLE 4** The resin uptake of H60, T400 and T92

<b>Foam</b>	<b>Series n=3</b>	<b>PVC H60</b>	<b>SAN T400</b>	<b>PET T92</b>
Before infusion Density (kg/m <sup>3</sup> )	Ave	61.36	74.31	103.1
	Std. dev	0.57	0.54	0.18
After Infusion Density (kg/m <sup>3</sup> )	Ave	94.27	107.92	144.93
	Std. dev	0.43	0.89	1.19
Resin uptake (kg/m <sup>2</sup> )	Ave	0.86	0.93	1.06
	Std. dev	0.01	0.01	0.01

**TABLE 5** Pore morphology data of H60, T400 and T92

Samples	Pore number	Pore size (mm)	Expansion ratio	Pore density (pores/cm <sup>3</sup> )
H60	38	0.43	13.8	$1.42 \times 10^5$
T400	35	0.47	23	$2.51 \times 10^5$
T92	47	0.40	15.07	$2.42 \times 10^5$